Journal of Power Sources 196 (2011) 9437–9444

Contents lists available at ScienceDirect

Journal of Power Sources

journal homepage: www.elsevier.com/locate/jpowsour

Effects of cathode gas diffusion layer design on polymer electrolyte membrane fuel cell water management and performance

Tak Cheung Yau [a], Massimiliano Cimenti [b], Xiaotao Bi [a,*], Jürgen Stumper [b]

[a] Department of Chemical and Biological Engineering, University of British Columbia, 2360 East Mall, Vancouver, BC V6T 1Z3, Canada
[b] Automotive Fuel Cell Cooperation Corporation, 9000 Glenlyon Parkway, Burnaby, BC V5J 5J8, Canada

ARTICLE INFO

Article history:
Received 11 May 2011
Received in revised form 30 June 2011
Accepted 1 July 2011
Available online 12 July 2011

Keywords:
Water management
PEMFC
Microporous layer

ABSTRACT

The effects of a microporous layer (MPL) on performance and water management of polymer electrolyte fuel cells are investigated. The presence of an MPL on the cathode side is found to slightly improve performance, although the voltage gain is less significant than that obtained by wetter reactants. The effect of the MPL on water management depends on the cathode inlet-gas humidity. Differences in water crossover rate are insignificant for wet cathode feed (RH = 75%), while they are significant for dry feed (RH = 25%). A model based on transport resistance of the MPL is proposed to explain the experimental trends observed. Modeling results suggest that the presence of the MPL on the cathode side causes a reduction of the water flux from the cathode catalyst layer to the flow channels, effectively promoting water back diffusion through the membrane. Higher cathode humidity reduces the driving force for water transport from the electrode to the gas channels, also reducing the importance of the water transport resistance due to the presence of the MPL.

1. Introduction

Performance is one of the key factors for the commercial success of polymer electrolyte membrane fuel cells (PEMFCs) as power supplies in automotive applications. Performance losses are typically categorized as kinetic, ohmic, and mass transport losses [1]. Ohmic and mass transports losses are related to water content in the membrane electrolyte assembly (MEA). Membrane conductivity and, in turn, ohmic losses depend on the water content in the membrane [2,3]. On the other hand, liquid water can partially saturate the pores in the cathode catalyst layer, reducing the accessibility of oxygen to the reaction sites. Therefore, the optimization of water management is important to improve PEMFC performance [4,5]. A useful parameter in this context is the water crossover flux, which is defined as the flux of water transported through the membrane. In the literature there are different conventions on the sign for water cross-over flux; here positive flux is defined as going from anode to cathode. Another parameter useful to characterize PEMFC water management is the water crossover coefficient (α), which is defined as the water crossover rate divided by the rate of water produced at the cathode by electrochemical reaction [6]. Understanding how water is transferred in a MEA can provide insight for improving water management to avoid cathode flooding but prevent membrane dehydration.

In the typical MEA design, microporous layers (MPLs) are added between the electrode and the gas diffusion layer (GDL) of both anode and cathode. The MPL is composed of a mixture of carbon powder and polytetrafluoroethylene (PTFE), and is characterized by porosity mainly in the micro- and meso-scales (2–50 nm in diameter). The MPL helps reduce the contact resistance between the electrode and GDL [1], and is expected to affect water management. Several research groups investigated the effect of the MPL on water crossover rate. Janssen and Overvelde performed water crossover measurements for MEAs with and without MPL [7], and found that water crossover rate was not significantly different at a current density of 0.4 A cm^{-2}, while it was lower for MEAs with MPL on the cathode side at 0.6 A cm^{-2}. Atiyeh et al. conducted similar experiments [8], and found that the presence of a MPL on the cathode side had negligible impact on overall water transfer at current densities lower than 0.7 A cm^{-2}. Kim et al. [9] found that MEAs with MPLs on both sides had higher water crossover rate compared to those with MPL on the cathode side only; they also noticed that more positive water crossover rates were measured in MEAs without MPL. To explain these observations they proposed that the MPL acts as a capillary barrier for water transport. Dai et al. performed experiments where dry air was fed to the cathode and liquid water to the anode [10]; they observed that when the MPL was present the water transport to the cathode channels was reduced if the air flow was larger than a certain value. To explain their results the authors proposed that at higher air-flows more water is driven out of the membrane leading to a higher capillary pressure in the micropores, and subsequently decreasing the effective water trans-

* Corresponding author. Tel.: +1 604 822 4408; fax: +1 604 822 6003.
E-mail address: xbi@chbe.ubc.ca (X. Bi).

0378-7753/$ – see front matter © 2011 Elsevier B.V. All rights reserved.
doi:10.1016/j.jpowsour.2011.07.002

Nomenclature

Symbols

A	cell active area (cm^2)
a	sulfonic acid group concentration ($1200\ mol\ m^{-3}$)
C	dimensionless concentration
F	Faraday's constant ($96{,}500\ C\ mol^{-1}$)
$\bar{I}$	average current density ($A\ cm^{-2}$)
J	molar flux ($mol\ cm^{-2}\ s^{-1}$)
$\bar{J}$	average molar flux ($mol\ cm^{-2}\ s^{-1}$)
$\dot{n}$	molar flow rate ($mol\ s^{-1}$)
P	partial pressure (kPa)
r	pore radius (m)
R	universal gas constant ($8.314\ J\ mol^{-1}\ K^{-1}$)
RH	relative humidity
T	temperature (K)
V_m	molar volume ($m^3\ mol^{-1}$)
y	mole fraction (wet basis)

Greek letters

α	water crossover coefficient
γ	interfacial water transport coefficient ($m\ s^{-1}$)
γ_C	cathode lumped water transport coefficient ($m\ s^{-1}$)
τ	liquid–vapour surface tension ($N\ m^{-1}$)
θ	contact angle

Subscripts

A	anode
cal	calibration
C	cathode
cc	cathode catalyst layer to channel
eqm	equilibrium
H_2O	water
in	inlet
m	membrane
MFC	mass flow controller for fuel cell feed
MFM	mass flow meter for dilution gas
out	outlet
pore	inside pore
sat	saturation
X	crossover (anode to cathode)

Abbreviations

CAM	capillary action model
EOD	electro-osmotic drag
GDL	gas diffusion layer
MEA	membrane electrode assembly
MPL	microporous layer
PEMFC	polymer electrolyte membrane fuel cell
RH	relative humidity
TRM	transport reduction model

port from the membrane to the GDL. Ye and Wang [11] published experimental results showing that a higher cathode GDL diffusivity leads to higher water crossover from anode to cathode.

The effect of the MPL on water crossover rate has also been addressed in several modeling studies. Weber and Newman [12] developed a model of water transport in PEMFCs. According to their simulation results the MPL on the cathode side increases the water flow from cathode to anode, effectively reducing cathode flooding as well as decreasing membrane resistance. Murahashi et al. [4] proposed a model of water management in a PEMFC that includes the effect of MPL capillary pressure; their modeling results indicated that when the MPL is present the water crossover coefficient is lower (i.e. less water flows to the cathode). On the other hand, other researchers proposed that the MPL helps removing water from the cathode catalyst layer without enhancing back diffusion through the membrane. According to Pasaogullari and Wang [13], the presence of a MPL enhances the removal of liquid water from the cathode and reduces the saturation levels in the diffusion media by inducing discontinuity in the porosity and surface properties between the MPL and the GDL. However, water transfer to/from the membrane was neglected in their model.

In summary, the effect of the MPL on water crossover is not yet clear. In this study we investigated the effects of a cathode-side MPL on water crossover rate at different humidities and current densities using a custom-designed tool described previously [6,14].

2. Experimental

2.1. Water crossover measurement equipment

The setup for measuring water crossover has been described previously [6,14]. To eliminate systematic errors from the different components of the measuring tool, a testing protocol that includes frequent calibration was developed. The water concentrations of a gas stream are continuously monitored by infrared sensors (Fig. 1). The humidification of the inlet gas streams is achieved using high-accuracy syringe pumps that inject a known flow rate of liquid water into a heated block where the vapour is mixed with a known flow rate of dry gas stream controlled by automated mass-flow controllers. During the 'normal' mode (Fig. 1(a)) the main set of syringe pumps provides the desired relative humidity (RH) to anode and cathode inlet streams, while the outlet vapour concentration from the fuel cell is measured. During the 'calibration' mode (Fig. 1(b)) a backup set of syringe pumps supplies the desired water flow to the fuel cell inlet streams, and the outlets streams from the cell are directed to a vented line. Meanwhile the infrared sensors are calibrated against the main set of syringe pumps.

The molar flux of water through the membrane is obtained from the water mass balance for both anode and cathode using the following equations:

$$\dot{n}_{H_2O,X,A} = \dot{n}_{H_2O,in,A} - \dot{n}_{H_2O,cal,A}\frac{y_{H_2O,out,A}}{y_{H_2O,cal,A}} \times \left(\frac{\dot{n}_{MFM,A} + \dot{n}_{MFC,A} - (\bar{I}A/2F)}{\dot{n}_{MFM,cal,A}}\right) \quad (1)$$

and

$$\dot{n}_{H_2O,X,C} = \dot{n}_{H_2O,cal,C} - \frac{y_{H_2O,out,C}}{y_{H_2O,cal,C}}\left(\frac{\dot{n}_{MFM,C} + \dot{n}_{MFC,C} - (\bar{I}A/4F)}{\dot{n}_{MFM,cal,C}}\right) - \dot{n}_{H_2O,in,C}\frac{\bar{I}A}{2F} \quad (2)$$

The average water crossover flux $\bar{J}_{H_2O}$ is defined by the water crossover rate per unit cell area:

$$\bar{J}_{H_2O} = \frac{\dot{n}_{H_2O,X,A}}{A} = \frac{\dot{n}_{H_2O,X,C}}{A} = \frac{\dot{n}_{H_2O,X}}{A} \quad (3)$$

This approach yields a more accurate determination of the crossover flux since all terms involved in the calculation are measured using the same equipment (i.e. same syringe pumps). Therefore the systematic errors of the equipment cancel out.

As reported by Yau et al. [14], the crossover rate obtained from the cathode signals (Eq. (2)) data may be affected by hydrogen crossover, so only the crossover rates obtained from the anode side (Eq. (1)) are reported here.

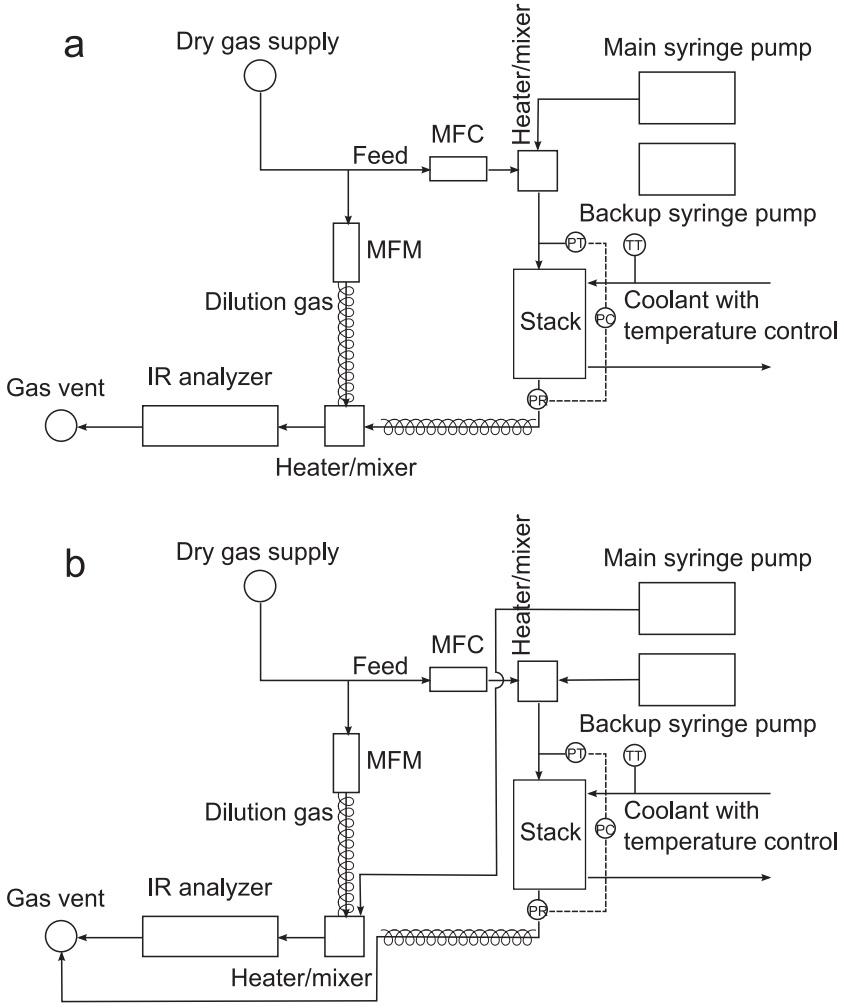

Fig. 1. Schematic diagram of the experimental setup. One side/electrode of the setup is shown. (a) Configuration for 'normal mode' measurements, when the water crossover rate for the fuel cell is measured. (b) Configuration for the 'calibration mode', when liquid water from the main syringe pump is fed directly to mix with the dilution gas from MFM and then analyzed by the infrared analyzer as a reference reading, while the backup pump provides humidified flow to maintain steady conditions at the cell. The outlet gases from the cell are purged to the vent.

2.2. MEA construction and operating conditions

Four MEAs with a nominal area of 50 cm^2 were prepared from catalyst coated membranes (Nafion NRE211) and Toray GDL coated with PTFE. Two of the MEAs had MPLs on both anode and cathode, and the other two had MPLs on the anode side only. Each pair was tested at identical conditions to verify the reproducibility.

The experimental conditions used in this study are summarized in Table 1. The effects of MPLs and the effects of differences in inlet RH between anode and cathode are addressed in this study. To minimize the effect of pressure on water crossover, both anode and cathode pressures were kept at 230 kPa (absolute). Each polarization curve was obtained by running the cell at 7 different current densities. To avoid possible effects of hysteresis, the order for different current densities in the polarization curve was randomized for each run. The dry gas flow rates were constant at all current densities.

3. Results and discussion

Fig. 2 shows the polarization curves for runs 1–8 (see Table 1). In these runs the anode inlet RH was kept constant (RHa = 75%) while the cathode inlet humidification changed (RHc = 25% or RHc = 75%). The results presented are the average from two different MEAs with

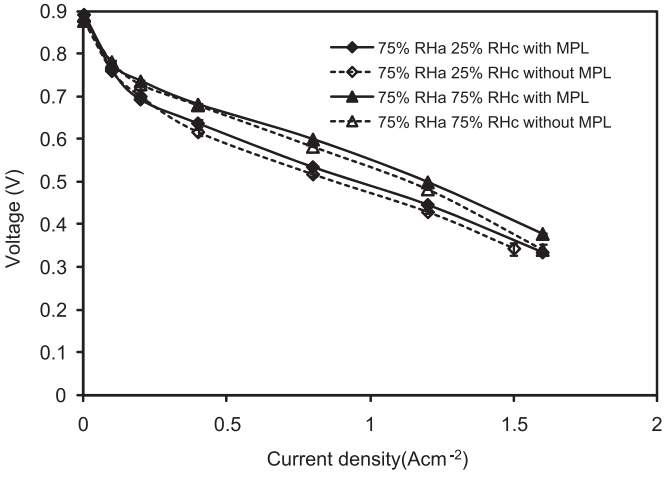

Fig. 2. Experimental polarization curves at constant fuel and oxidant flow rates. Results are the average from two replicates. MEA construction and cathode RH are as indicated. $T = 70\,^{\circ}C$, $P_A = 230$ kPa, $P_C = 230$ kPa, $RH_{in,A} = 75\%$, H_2 flow rate = 4.46×10^{-3} mol s^{-1}, N_2 flow rate = 2.94×10^{-3} mol s^{-1}, O_2 flow rate = 7.81×10^{-4} mol s^{-1}. Error bars indicate the difference in readings between the two replicates; solid symbols may cover the whole error bar.

Table 1
Nominal conditions reported in this work.

Run	MEA #	With MPL	Cell temperature (°C)	Anode pressure (kPa)	Cathode pressure (kPa)	H_2 flow rate (mol s^{-1})	N_2 flow rate (mol s^{-1})	O_2 flow rate (mol s^{-1})	Anode RH (%)	Cathode RH (%)
1	1	No	70	230	230	4.46×10^{-3}	2.94×10^{-3}	7.81×10^{-4}	75	25
2	1	No	70	230	230	4.46×10^{-3}	2.94×10^{-3}	7.81×10^{-4}	75	75
3	2	No	70	230	230	4.46×10^{-3}	2.94×10^{-3}	7.81×10^{-4}	75	25
4	2	No	70	230	230	4.46×10^{-3}	2.94×10^{-3}	7.81×10^{-4}	75	75
5	3	Yes	70	230	230	4.46×10^{-3}	2.94×10^{-3}	7.81×10^{-4}	75	25
6	3	Yes	70	230	230	4.46×10^{-3}	2.94×10^{-3}	7.81×10^{-4}	75	75
7	4	Yes	70	230	230	4.46×10^{-3}	2.94×10^{-3}	7.81×10^{-4}	75	25
8	4	Yes	70	230	230	4.46×10^{-3}	2.94×10^{-3}	7.81×10^{-4}	75	75
9	1	No	70	230	230	4.46×10^{-3}	2.94×10^{-3}	7.81×10^{-4}	25	25
10	1	No	70	230	230	4.46×10^{-3}	2.94×10^{-3}	7.81×10^{-4}	25	75
11	3	Yes	70	230	230	4.46×10^{-3}	2.94×10^{-3}	7.81×10^{-4}	25	25
12	3	Yes	70	230	230	4.46×10^{-3}	2.94×10^{-3}	7.81×10^{-4}	25	75
13	1	No	70	230	230	4.46×10^{-3}	2.94×10^{-3}	7.81×10^{-4}	75	100
14	2	No	70	230	230	4.46×10^{-3}	2.94×10^{-3}	7.81×10^{-4}	75	100
15	3	Yes	70	230	230	4.46×10^{-3}	2.94×10^{-3}	7.81×10^{-4}	75	100
16	4	Yes	70	230	230	4.46×10^{-3}	2.94×10^{-3}	7.81×10^{-4}	75	100

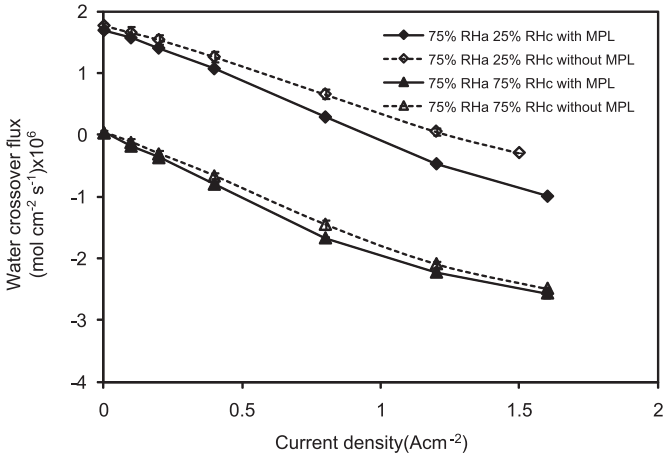

Fig. 3. Water crossover flux (measured from anode) against current density. Negative values indicate water transfer from cathode back to anode. Results are the average from two replicates. MEA construction and cathode RH are as indicated. $T = 70\,^{\circ}C$, $P_A = 230$ kPa, $P_C = 230$ kPa, $RH_{in,A} = 75\%$, H_2 flow rate $= 4.46 \times 10^{-3}$ mol s^{-1}, N_2 flow rate $= 2.94 \times 10^{-3}$ mol s^{-1}, O_2 flow rate $= 7.81 \times 10^{-4}$ mol s^{-1}. Error bars indicate the difference in readings between the two replicates; solid symbols may cover the whole error bar.

the same design. Reproducibility was satisfactory with a voltage variation smaller than 31 mV at all current densities.

The performance difference between MEAs with and without MPL was negligible for current densities < 0.1 A cm^{-2} at both RH conditions. Thus, feed humidification and the addition of the MPL has little effect on the kinetics of the electrochemical reaction. From 0.5 to 1.2 A cm^{-2}, the cell voltage is higher for the MEAs with MPL. As expected, the effect of the cathode inlet humidification is significant for both designs at current densities higher than 0.1 A cm^{-2}, indicating lower ohmic losses in the membrane and cathode layer as a result of the increased water concentration in the ionomer. Mass transport loss appears minimal from 0 to 1.6 A cm^{-2} as suggested by the absence of a characteristic 'shoulder' shaped drop in voltage on the polarization curve.

Fig. 3 shows the water crossover flux corresponding to the polarization curves of Fig. 2, which is calculated from the water concentration measured at anode outlet. The water crossover fluxes were acquired at different current densities, from 0 to 1.6 A cm^{-2}, at the same time as the polarization curve in Fig. 2. Again the two replicates show good reproducibility with a sample-to-sample difference in water crossover flux smaller than 1.74×10^{-7} mol cm^{-2} s^{-1} (equivalent to a current of 34 mA cm^{-2}). The intercepts in Fig. 3 are indicative of the RH gradients across the membrane: for the case with different RH at cathode and anode (RHc = 25% and RHa = 75%) the intercept is positive (i.e. positive water crossover flux) because there is a gradient in water concentration between the two sides of the membrane, which drives water from anode to cathode; when the inlet RH is the same (RHc = RHa = 75%) the intercept is zero. At positive current densities water produced at the cathode generates a water concentration gradient across the membrane, causing back-diffusion of water to the anode (i.e. more negative water crossover flux). The trends in water crossover flux against the current density are linear up to approximately 1.5 A cm^{-2} for the condition with 25% cathode RH and up to 1.2 A cm^{-2} for 75% cathode RH. The curves for 75% cathode RH are slightly deflected upwards at higher current densities.

By comparing the water crossover trends for MEAs with and without MPL, it can be seen that the presence of the MPL causes the slope of the water crossover flux to be more negative, particularly for the runs with RHc = 25%. Therefore, at these operating conditions the presence of the MPL enhances back diffusion of product water to the anode. An argument derived from a mass balance at the

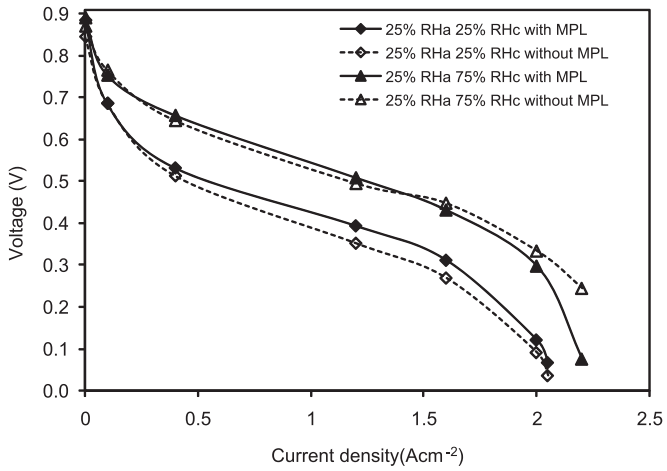

Fig. 4. Experimental polarization curves at constant fuel and oxidant flow rates. Results are the average from two replicates. MEA construction and cathode RH are as indicated. $T = 70\,^{\circ}C$, $P_A = 230\,kPa$, $P_C = 230\,kPa$, $RH_{in,A} = 25\%$, H_2 flow rate $= 4.46 \times 10^{-3}\,mol\,s^{-1}$, N_2 flow rate $= 2.94 \times 10^{-3}\,mol\,s^{-1}$, O_2 flow rate $= 7.81 \times 10^{-4}\,mol\,s^{-1}$.

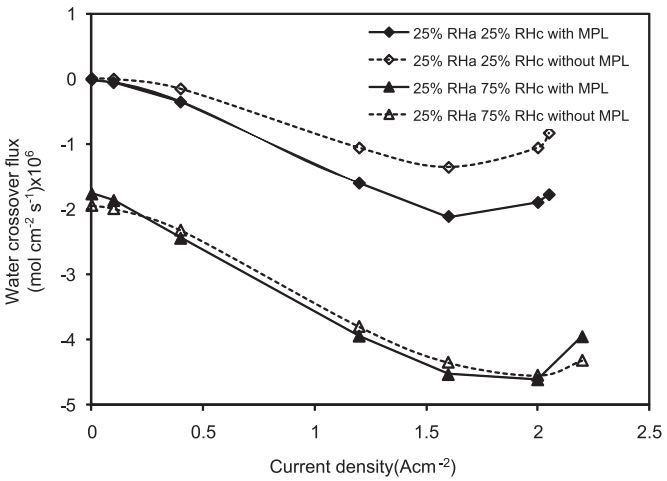

Fig. 5. Water crossover flux (measured from anode) against current density. Negative values indicate water transfer from cathode back to anode. MEA construction and cathode RH are as indicated. $T = 70\,^{\circ}C$, $P_A = 230\,kPa$, $P_C = 230\,kPa$, $RH_{in,A} = 25\%$, H_2 flow rate $= 4.46 \times 10^{-3}\,mol\,s^{-1}$, N_2 flow rate $= 2.94 \times 10^{-3}\,mol\,s^{-1}$, O_2 flow rate $= 7.81 \times 10^{-4}\,mol\,s^{-1}$.

cathode catalyst layer proposed in Ref. [14] is used to estimate the fraction of water generated at the cathode that back-diffuses to the anode and exits the cell through the anode channels. The simulation results for the runs with inlet RHc = 25% indicate that 33.7% of the water generated by electrochemical reaction flows to the anode in the MEAs with MPL, while for the MEAs without MPL it is 27.4%. For the case with equal inlet RH of 75%, the calculations indicate that similar fractions of product water flow to the anode regardless of the presence of the MPL; 34.9% without MPL, and 37.4% with MPL. This estimate agrees with the experimental results of Fig. 3. These experimental results are consistent also with the findings of Atiyeh et al. [8], who observed insignificant changes in water crossover rates for anode and cathode humidities of 60% and 100%, respectively. In contrast, results by Kim et al. [9] showed that MPL on the cathode side enhanced water transfer back to the anode side even for saturated cathode feeds.

Fig. 4 shows the polarization curves obtained for RHa = 25%, and RHc = 25 or 75% (runs 9–12, in Table 1). The performance improves slightly for MEA with MPL, mainly in the ohmic region (0.5–1.5 A cm^{-2}). However, for current densities higher than 1.5 A cm^{-2} this performance gain decreases, and the MEA without MPL performs better for RHc = 75%. The 'shoulder' observed in the polarization curve for the MEA with MPL and for RHc = 75% could be caused by oxygen diffusion limitations. This feature is less evident in the polarization curve measured for the same MEA at 25% RH on both sides.

Fig. 5 shows the water crossover flux as a function of the current density corresponding to the polarization curves of Fig. 4. The effects of the MPL on water crossover depend again on the cathode inlet RH, as in Fig. 3. For current densities larger than 1.6 A cm^{-2}, the water flux from cathode to anode decreases with increasing current. This behaviour could be caused by saturation of the membrane at the interface with the cathode. After the ionomer at that interface is saturated, local water concentration cannot increase any further and the driving force for back diffusion of water is effectively reduced. This hypothesis can possibly explain the plateau in the water crossover flux observed between 1.6 and 2 A cm^{-2}. On the other hand, the water flux due to electro-osmotic drag increases with increasing current density, possibly explaining the observed bending upwards of the curve.

Fig. 6 shows the polarization curves obtained for RHa = 75% and RHc = 100%. Up to 1.7 A cm^{-2} the polarization curve for the MEAs without MPL is not significantly different from the one measured at RHa = RHc = 75% (same RH at both sides) and shown in Fig. 2. On the other hand, the polarization curve for the MEAs with MPL shows an evident mass-transport shoulder (already observed for RHa = 25%, RHc = 75% in Fig. 4). The plot of the water crossover flux versus the current density corresponding to the polarization curves of Fig. 6 is shown in Fig. 7. Similar to the previous runs at RHc = 75% (Fig. 5), the MPL has no significant effect on water crossover fluxes. The water content and distribution in the membrane is likely similar for both MEA types, given that the inlet humidification is the same and the water crossover flux is also the same. The performance of the MEAs with MPL at this condition (RHc = 100%) is the highest of all runs, and it is significantly higher than that measured for MEA without MPL at the same conditions, particularly in the ohmic region of the polarization curve. It is possible that the difference in performance within the ohmic region between the two types of MEAs is caused by differences in contact resistance at the cathode/GDL interface.

A common hypothesis found in the literature [4,9] to explain the effects of the MPL on water management is that the MPL effectively decreases the saturation pressure of water vapour by means

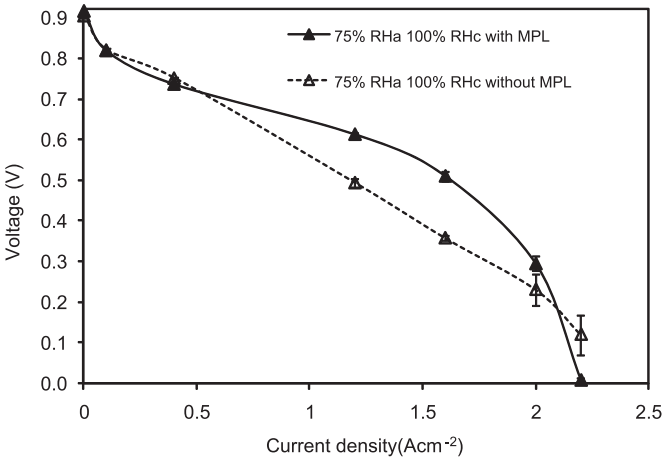

Fig. 6. Experimental polarization curves at constant fuel and oxidant flow rates. Results are the average from two replicates. MEA construction is as indicated. $T = 70\,^{\circ}C$, $P_A = 230\,kPa$, $P_C = 230\,kPa$, $RH_{in,A} = 75\%$, $RH_{in,C} = 100\%$, H_2 flow rate $= 4.46 \times 10^{-3}\,mol\,s^{-1}$, N_2 flow rate $= 2.94 \times 10^{-3}\,mol\,s^{-1}$, O_2 flow rate $= 7.81 \times 10^{-4}\,mol\,s^{-1}$. Error bars indicate the difference in readings between the two replicates; solid symbols may cover the whole error bar.

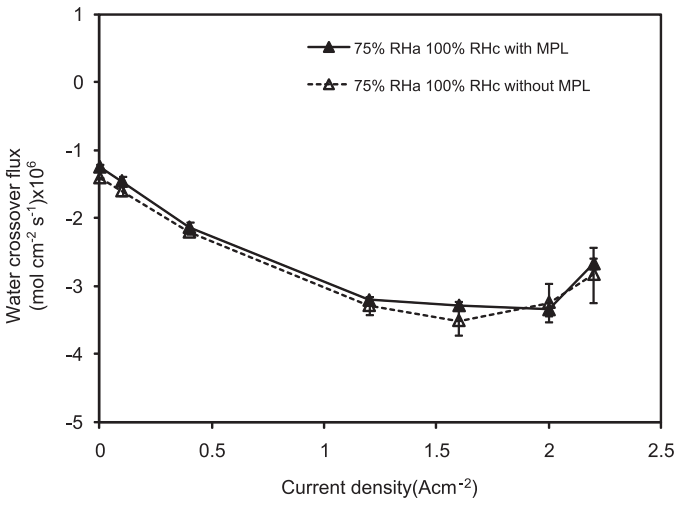

Fig. 7. Water crossover flux (measured from anode) against current density. Negative values indicate water transfer from cathode back to anode. Results are the average from two replicates. MEA construction is as indicated. $T = 70\,^{\circ}C$, $P_A = 230$ kPa, $P_C = 230$ kPa, $RH_{in,A} = 75\%$, $RH_{in,C} = 100\%$, H_2 flow rate $= 4.46 \times 10^{-3}$ mol s^{-1}, N_2 flow rate $= 2.94 \times 10^{-3}$ mol s^{-1}, O_2 flow rate $= 7.81 \times 10^{-4}$ mol s^{-1}. Error bars indicate the difference in readings between the two replicates; solid symbols may cover the whole error bar.

of capillary action (capillary action model, CAM). This is described by the Kelvin equation, which relates the actual vapour pressure in a hydrophobic pore of radius r and contact angle θ ($P_{sat,pore}$) to the saturation pressure (P_{sat}) [15]:

$$P_{sat,pore} = P_{sat} \cdot \exp\left(-\frac{2 \cdot \tau \cdot \cos\ \theta \cdot V_m}{r \cdot R \cdot T}\right) \quad (4)$$

The average pores size in a MPL is much smaller compared to the carbon paper in the GDL. According to the above equation, the presence of a MPL on the cathode side should cause a lower saturation pressure close to the cathode/membrane interface. That is, for the same inlet conditions the actual RH (and water vapour activity) near to the MPL is higher, thereby increasing the local concentration of water in the ionomer of the cathode, also increasing the water concentration gradient across the membrane. This should result in the effective increase of water back-diffusion. In theory this effect is present regardless of the current density, thus there should be a negative water crossover flux even at zero current when anode and cathode inlet RH is the same. Experimental evidence against this hypothesis can be observed in Fig. 3, where the intercepts of the water crossover flux corresponding to zero current are close to zero both MEA types with and without MPL.

An alternative hypothesis is proposed to explain the MPL effects on water management through hydraulic action. Based on modeling results, Weber and Newman [12] and Baghalha et al. [16] proposed that a decrease in hydraulic permeability towards the cathode side due to the presence of a MPL will drive water towards the anode side while the cathode catalyst layer is saturated at low current densities regardless of inlet RH [16]. However, the results shown in Fig. 7 for saturated cathode feeds seem to contradict this hypothesis, since the presence/absence of the MPL in the above experiments did not have a significant effect on the water crossover flux.

Another possible explanation of the role of the MPL on water management is that it reduces the transport of water from the cathode layer to the cathode channels by decreasing the effective transport coefficient for water vapour through the GDL (transport reduction model, TRM). As a result, a larger fraction of the water generated has to move towards the anode side, leading to a more negative water crossover flux. When there is no RH gradient across anode and cathode channels and there is no load, any changes in water transport resistance at the cathode GDL have no effect, which is consistent with the experimental findings in this paper.

The TRM described above is also consistent with the experimental results showing similar water crossover fluxes between MEAs with and without MPL at high cathode inlet RH. Following Refs. [17,18], it is assumed that water is generated by the electrochemical reaction at the cathode membrane interface. The water removed from the cathode/membrane interface is proportional to the difference between the actual membrane water content at the interface $C_{H_2O,C}$ and the water content in equilibrium with the water vapour at the interface $C_{H_2O,eqm}$ through an interfacial transport coefficient γ [17,18]:

$$J_{H_2O} = a \cdot \gamma \cdot (C_{H_2O,C} - C_{H_2O,eqm}) \quad (5)$$

This is equal to the flux from the cathode membrane interface to the cathode channel only when there is no transport resistance of water vapour between the interface and the channel [18]. Here it is assumed that the diffusion of water vapour between the cathode membrane interface and the channel can be incorporated with membrane interfacial water transport described above, such that an equivalent equation can be written as:

$$J_{H_2O,cc} = a \cdot \gamma_C \cdot (C_{H_2O,C} - C_{H_2O,eqm,C}) \quad (6)$$

where $C_{H_2O,eqm,C}$ is the water concentration at equilibrium with the *cathode channel humidity*, and γ_C is a lumped transport coefficient accounting for both membrane interfacial transport and diffusion between the membrane interface and the cathode channel. Any diffusion resistance between the membrane interface and the cathode channel would therefore be reflected by a smaller value of γ_C compared to γ.

The diffusion resistance from the cathode channel to the cathode membrane interface increases when the MPL is added to the cathode GDL, leading to a smaller transport coefficient γ_C. When the cathode RH is high, the equilibrium concentration of water ($C_{H_2O,eqm,C}$) also increases according to the equation proposed by Springer et al. [19]. At a given current density, the water reaching the cathode/membrane interface by electro-osmotic drag and water generated by electrochemical reaction is the same independent of the presence of the MPL. Thus, the steady-state water concentration of the cathode interface ($C_{H_2O,C}$) should not change significantly. Subsequently, the driving force for the flow of water from the cathode interface to the cathode channel ($C_{H_2O,C} - C_{H_2O,eqm,C}$) decreases, and differences in flux for different transport coefficient γ_C become less significant. The trends expected for the TRM are consistent with a weaker effect of the MPL on increasing back-diffusion at high cathode relative humidity.

As an illustration of the capillary action model (CAM) and the transport reduction model (TRM), Eqs. (4) and (6) are independently incorporated into the fuel cell model by Berg et al. [18]. The additional model parameters introduced by CAM are the pore radius r and the contact angle θ, while the TRM introduces the cathode water transport coefficient γ_C as the additional parameter. The parameters for the original model without MPL are obtained by fitting the polarization and water crossover rate data simultaneously for runs 1–4. The additional parameters for CAM and TRM are found by fitting the data for runs 5–8. The best-fit pore radius in CAM is found to be 1.0×10^{-8} m assuming a contact angle of 140° [20], which is of the same order of magnitude as the pore size in typical microporous layers measured by mercury porosimetry [20,21]. The best-fit for γ_C in the TRM is found to be 25.8% smaller for the MEAs without MPL. This is consistent with the assumption that the MPL reduces water transport from the cathode layer to the channel.

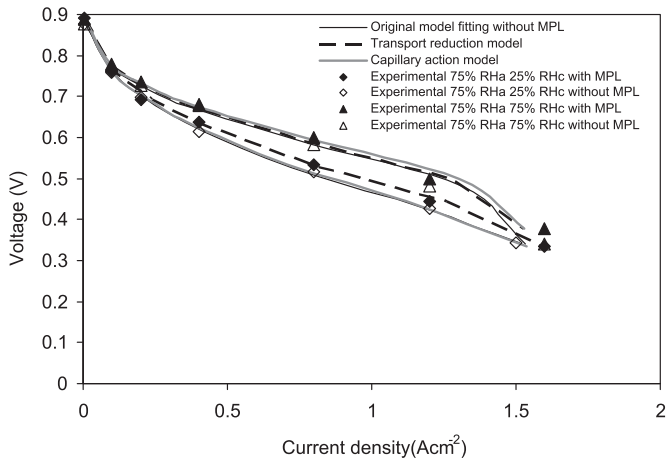

Fig. 8. Fitting results on the polarization curves using different models for the action of the MPL. The experimental data are the same as in Fig. 2. The original Berg model (solid black lines) was used to fit for data without MPL, the TRM (dotted lines) and CAM (solid grey lines) were used to fit the data with MPL.

According to the fitting results shown in Fig. 8, both models capture the voltage gain observed for the MEA with MPL under the conditions in runs 1–8 (Figs. 2 and 3). However, as shown in Fig. 9, the CAM model requires a negative water crossover flux for the run with the equal inlet RH, which is not consistent with the observations discussed earlier. For the run with 25% cathode and 75% anode inlet RH, the CAM underestimates the effect of back diffusion because the predicted water crossover is less negative.

The best-fit pore radius of 1.0×10^{-8} m leads to an increase in RH at the cathode membrane interface from 25% to 26.7%. As a result, CAM hardly captures the large increase in back diffusion at 25% cathode RH observed in the experiments (compare solid symbols to grey line in Fig. 9). On the other hand, TRM gives a better fit in water crossover (compare solid symbols to dashed black line in Fig. 9). The change in slope of the water crossover flux against current density at 25% cathode RH is more evident for TRM fit compared to the CAM fit. For the same degrees of freedom (i.e. number of fitting parameter), the TRM model gives a better fit to the experimental results. In summary, the effect of the MPL on water management is possibly related to the increase in water transport resistance between the cathode electrode and the cathode channel, and this effect is less significant when the cathode channel RH is close to saturation because the driving force for water removal decreases. Since

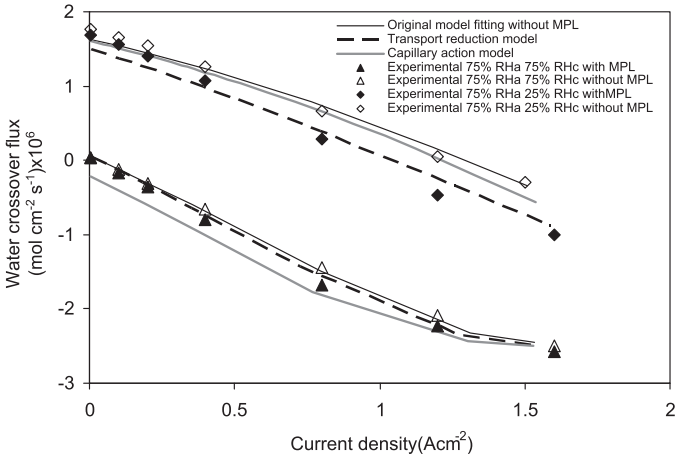

Fig. 9. Fitting results on water crossover using different models for the action of the MPL. The experimental data are the same as in Fig. 3. The original Berg model (solid black lines) was used to fit for data without MPL, the TRM (dotted lines) and CAM (solid grey lines) were used to fit the data with MPL.

the experiments in this article involve only one type of MPL, more tests on MPLs with different binder and carbon compositions may be necessary to generalize the findings listed above.

There are other physical phenomena that could affect the experimental observations, such as temperature gradients in the MEA in through-plane direction. Owejan et al. [20] demonstrated that the temperature gradient between the cathode catalyst layer and the cathode channels may be sufficient to drive water diffusion towards the cathode channels. Further investigations are required to elucidate the temperature effects in the transport mechanism of water across the MPL.

4. Conclusions

The effects of a MPL on performance and water management of PEMFC were investigated. Adding the MPL increases the cell voltage under the same current density, except for the case of 100% cathode RH. However, the performance increase is larger when the inlet RH is increased than when the MPL is added. For the cases of wet cathode inlet a mass transport 'shoulder' was observed for MEAs with MPL at high current densities. This effect is less evident for MEAs without MPL. At moderate current densities the water crossover flux decreases linearly with increasing the current, while at high current densities the trend is inverted, possibly indicating water saturation at the cathode catalyst layer/membrane interface. The presence of the MPL in the cathode GDL increases back diffusion of water to the anode channels only at low cathode RH (25%), regardless of RH gradient between anode and cathode. To explain the experimental observations it is proposed that the effect of the MPL on water management is related to the increase in the transport resistance from the cathode catalyst layer to the cathode channels, which effectively increases water back-diffusion to the anode. At high cathode RH the driving force for water removal from the cathode electrode to the cathode channels decreases, and the effects of the MPL on transport reduction are less evident. Other physical processes, such as capillary effects and reduction of hydraulic conductivity caused by the presence of the MPL, are not consistent with the experimental observations. However, through-plane temperature gradients in the MEA might contribute to the observed trends of the water crossover flux at high current densities.

Acknowledgement

The authors would like to thank Dr. Edward Hillstrom at Automotive Fuel Cell Cooperation Corporation for his useful discussion on this article.

References

[1] F. Barbir, PEM Fuel Cells: Theory and Practice , Academic Press, Burlington, 2005.
[2] T. Zawodzinski, T. Springer, J. Davey, R. Jestel, C. Lopez, J. Valerio, S. Gottesfeld, Journal of the Electrochemical Society 140 (1993) 1981–1985.
[3] T. Zawodzinski, C. Derouin, S. Radzinski, R. Sherman, V. Smith, T. Springer, S. Gottesfeld, Journal of the Electrochemical Society 140 (1993) 1041–1047.
[4] T. Murahashi, M. Naiki, E. Nishiyama, Journal of Power Sources 162 (2006) 1130–1136.
[5] G. Lu, F. Liu, C. Wang, Journal of Power Sources 164 (2007) 134–140.
[6] P. Sauriol, D. Nobes, X. Bi, J. Stumper, D. Jones, D. Kiel, Journal of Fuel Cell Science and Technology 6 (2009), 041014.
[7] G. Janssen, M. Overvelde, Journal of Power Sources 101 (2001) 117–125.
[8] H. Atiyeh, K. Karan, B. Peppley, A. Phoenix, E. Halliop, J. Pharoah, Journal of Power Sources 170 (2007) 111–121.
[9] T. Kim, S. Lee, H. Park, International Journal of Hydrogen Energy 35 (2010) 8631–8643.
[10] W. Dai, H. Wang, X. Yuan, J. Martin, J. Shen, Z. Luo, M. Pan, Journal of Power Sources 188 (2009) 122–126.
[11] X. Ye, C. Wang, Journal of the Electrochemical Society 154 (2007) B683–B686.
[12] A. Weber, J. Newman, Journal of the Electrochemical Society 152 (2005) A677–A688.

[13] U. Pasaogullari, C.Y. Wang, Electrochimica Acta 49 (2004) 4359–4369.
[14] T. Yau, P. Sauriol, X. Bi, J. Stumper, Journal of the Electrochemical Society 157 (2010) B1310–B1320.
[15] A. Johnson, Colloids Surfaces A: Physicochemical and Engineering Aspects 202 (2002) 33–39.
[16] M. Baghalha, M. Eikerling, J. Stumper, 218th ECS Meeting, 2010.
[17] R. Bird, W. Stewart, E. Lightfoot, Transport Phenomena Revised , 2nd ed., John Wiley & Sons, New York, 2007.
[18] P. Berg, K. Promislow, J. St Pierre, J. Stumper, B. Wetton, Journal of the Electrochemical Society 151 (2004) A341–A353.
[19] T. Springer, T. Zawodzinski, S. Gottesfeld, Journal of the Electrochemical Society 138 (1991) 2334–2342.
[20] J.P. Owejan, J.E. Owejan, W.B. Gu, T.A. Trabold, T.W. Tighe, M.F. Mathias, Journal of the Electrochemical Society 157 (2010) B1456–B1464.
[21] S. Park, J.W. Lee, B.N. Popov, Journal of Power Sources 163 (2006) 357–363.